



OPEN

SUBJECT AREAS:  
LIGHT RESPONSES  
PROTEIN-PROTEIN INTERACTION  
NETWORKSReceived  
1 May 2014Accepted  
29 September 2014Published  
22 October 2014Correspondence and  
requests for materials  
should be addressed to  
G.W. (gcwang@qdio.  
ac.cn)

# Quantitative proteomic analysis of thylakoid from two microalgae (*Haematococcus pluvialis* and *Dunaliella salina*) reveals two different high light-responsive strategies

Wenhui Gu<sup>1</sup>, Huan Li<sup>1,2</sup>, Peipei Zhao<sup>1,2</sup>, Ruixue Yu<sup>3</sup>, Guanghua Pan<sup>3</sup>, Shan Gao<sup>1</sup>, Xiujun Xie<sup>1</sup>, Aiyu Huang<sup>1</sup>, Linwen He<sup>1</sup> & Guangce Wang<sup>1</sup><sup>1</sup>Key Laboratory of Experimental Marine Biology, Institute of Oceanology, Chinese Academy of Sciences, 7 Nanhai Road, 266071 Qingdao, China, <sup>2</sup>University of Chinese Academy of Sciences, 100049 Beijing, China, <sup>3</sup>College of Marine Science and Engineering, Tianjin University of Science and Technology, 300457 Tianjin, China.

Under high light (HL) stress, astaxanthin-accumulating *Haematococcus pluvialis* and  $\beta$ -carotene-accumulating *Dunaliella salina* showed different responsive patterns. To elucidate cellular-regulating strategies photosynthetically and metabolically, thylakoid membrane proteins in *H. pluvialis* and *D. salina* were extracted and relatively quantified after 0 h, 24 h and 48 h of HL stress. Proteomic analysis showed that three subunits of the cytochrome *b<sub>6</sub>/f* complex were greatly reduced under HL stress in *H. pluvialis*, while they were increased in *D. salina*. Additionally, the major subunits of both photosystem (PS) II and PSI reaction center proteins were first reduced and subsequently recovered in *H. pluvialis*, while they were gradually reduced in *D. salina*. *D. salina* also showed a greater ability to function using the xanthophyll-cycle and the cyclic photosynthetic electron transfer pathway compared to *H. pluvialis*. We propose a reoriented and effective HL-responsive strategy in *H. pluvialis*, enabling it to acclimate under HL. The promising metabolic pathway described here contains a reorganized pentose phosphate pathway, Calvin cycle and glycolysis pathway participating in carbon sink formation under HL in *H. pluvialis*. Additionally, the efficient carbon reorientation strategy in *H. pluvialis* was verified by elevated extracellular carbon assimilation and rapid conversion into astaxanthin.

A high light (HL) level is a commonly occurring environmental stress for both plants and photosynthetic algae in nature. For plants, photoacclimation strategies at multiple levels are employed to prevent photo-damage<sup>1</sup>, including visible leaf reorientation and chloroplast avoidance movement<sup>2–4</sup>, with short-term state transitions being initiated in less than seconds and long-term cellular photoacclimation that spans from hours to days<sup>5–7</sup>. For photosynthetic microalgae, prevention of photodamage at the cellular level is challenging compared to in higher plants, due to their unicellular structure. *Haematococcus pluvialis* is a green microalgae that exhibits HL tolerance accompanied with carotenogenesis<sup>8</sup>, predominantly the synthesis of the *keto*-carotenoid astaxanthin. Another unicellular green microalgae, *Dunaliella salina*, also accumulates carotenoids under stress stimulation and predominantly  $\beta$ -carotene under HL stress. Over the years, the two microalgae have been extensively investigated for their commercial applications in carotenoid production, in which HL was also widely applied. Although similar to each other, they have never been comparatively studied with respect to their thylakoid membrane proteomics during photoacclimation.

Both photoinhibition and photoacclimation involve a number of proteins in plants and microalgae<sup>9–11</sup>. Most noticeably, thylakoid membrane proteins are vulnerable to photodamage and vary greatly under HL stress<sup>9</sup>. Knowledge regarding the thylakoid membrane composition and alterations in response to HL stress could provide information on photosynthetic mechanisms. For *H. pluvialis*, photoacclimation and photoprotection mechanism research focuses mainly on the scavenging of HL-induced oxidants by astaxanthin<sup>12–14</sup>. It is a widely accepted theory that astaxanthin has multiple protective functions in *H. pluvialis* cells when subjected to HL-

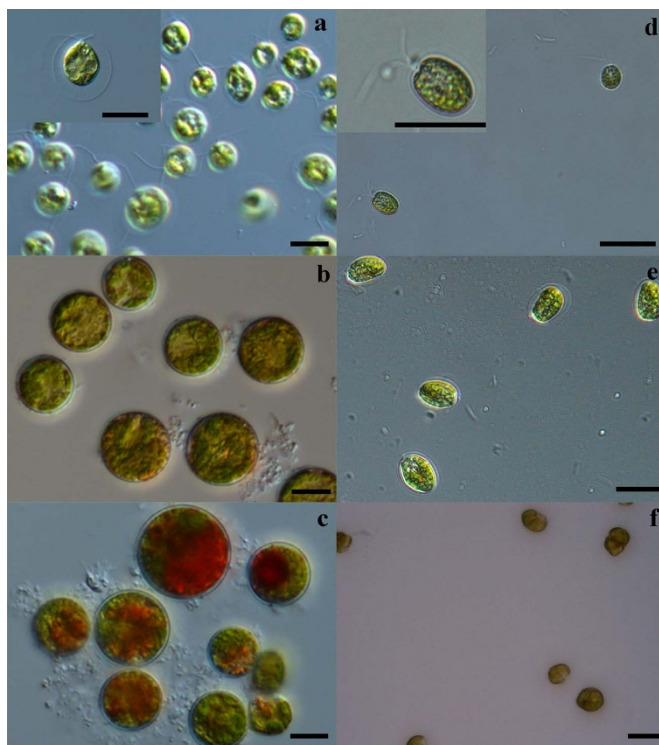


**Figure 1** | Cell morphology variation in two microalgae during different stages of high light (HL) stress: (a), *Haematococcus pluvialis* cells prior to HL stress (enlargement shows the two flagella); (b), *H. pluvialis* cells after 24 h of HL stress; (c), *H. pluvialis* cells after 48 h of HL stress; (d), *Dunaliella salina* cells prior HL stress (enlargement shows the two flagella); (e), *D. salina* cells after 24 h of HL stress; (f), *D. salina* cells after 48 h of HL stress.

induced photooxidative stress<sup>8</sup>. Additionally, cells with a higher astaxanthin level were shown to have a higher survival rate<sup>15,16</sup>. However, astaxanthin accumulation was also believed to be a byproduct of photodamage prevention rather than a direct substrate<sup>14</sup>. An alternative approach of determining how *H. pluvialis* acclimates under HL is to focus on the photosynthetic protein alterations. Previous research found that nutrient starvation combined with HL stress caused thylakoid polypeptide alterations<sup>9</sup> and that astaxanthin-rich cells showed a down-regulation of *cytochrome f* for protective purposes<sup>16</sup>. The low temperature fluorescence of the thylakoid membrane showed that cells tend to redistribute the absorbed light energy to acclimate<sup>10</sup>. To provide comprehensive and direct proof of the photoacclimation pattern, the photosynthetic proteins must be quantitatively analyzed.

Taking the protective role of astaxanthin and its biosynthesis process into consideration, the photoacclimation in *H. pluvialis* will be difficult to analyze. Additionally, there is the challenge of establishing a non-astaxanthin-accumulating *H. pluvialis* mutant. As reviewed by Lemoine and Schoefs<sup>8</sup>, in the two proposed astaxanthin biosynthesis phases,  $\beta$ -carotene is the essential precursor molecular and the *de novo* synthesis of  $\beta$ -carotene is required for prolonged astaxanthin accumulation<sup>17</sup>. Consequently, it would be ideal to find a comparable organism that shows  $\beta$ -carotene but not astaxanthin accumulation under HL stress. Fortunately, as an extensively investigated microalga, *D. salina* has the ability to accumulate  $\beta$ -carotene under HL stress<sup>18</sup> and, together with *H. pluvialis*, belongs to the Volvocales<sup>19</sup>.

The aim of the present work is to provide a depiction of the photosynthetic protein variation at the thylakoid proteomic level in the two microalgae, *H. pluvialis* and *D. salina*. The widely applied gel-based approach for comparative proteomic research, regular 2-D PAGE or 2-D DIGE, were not applicable to achieve this goal due to

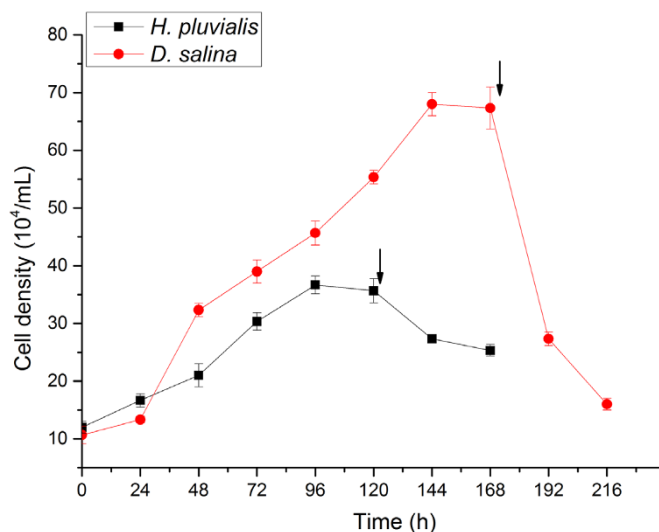


**Figure 2** | Cell density variation in two microalgae prior to and after high light (HL) stress. Arrow indicates the point at which HL stress was imposed.

their poor resolution of membrane proteins<sup>20</sup>. In recent years, advancements in high-throughput highly sensitive mass spectrometry (MS) instrumentation has enabled a gel-free approach as an alternative technique for protein differential analysis. An HPLC-coupled tandem MS instrumentation provides advantages for thylakoid membrane protein separation and identification<sup>21</sup>. In this work, we employed the HPLC-MS-based label-free technique for thylakoid membrane proteomic quantitation, which has been proved to be both reliable and cost-effective<sup>22</sup>.

## Results

### Cell morphology, growth and pigment variations under HL stress.

Both *H. pluvialis* and *D. salina* cells are biflagellated (Figure 1 a, d, respectively) and actively swimming in medium prior to HL stress. And loss of flagella was observed in both *H. pluvialis* and *D. salina* at 24 h of HL stress (Figure 1 b, e, respectively). A significant decrease in cell density was observed in the two algae under HL stress (Figure 2). The cell density of *H. pluvialis* decreased by 40.78%, while that of *D. salina* decreased by 76.11% after 48 h of HL stress.

HL effects on pigment composition were quite similar in *H. pluvialis* and *D. salina* as shown in Table 1 (HPLC separation results are provided in supplementary data, Figure S1 and S2). The ratio of chlorophyll *b* to chlorophyll *a* and the level of neoxanthin were relatively insensitive to HL in the two microalgae. The xanthophyll-cycle pigments varied synchronously in the two algae. Violaxanthin was noted to be decreased, while antheraxanthin and zeaxanthin were noted to be significantly increased. And the total amount of xanthophyll-cycle pigments (the sum of violaxanthin, antheraxanthin and zeaxanthin) increased during the course of HL stress. As an indicator of the xanthophyll-cycle, the conversion ratio (AZ/VAZ) significantly increased along with the HL stress in both algae (Table 1).

### Imbalance of electron transport rate between PSI and PSII.

HL had a significant effect on both PSI and PSII activity (Figure 3). However, for *H. pluvialis* and *D. salina*, there were different patterns of response to HL, as indicated by the variance levels of ETR(I), ETR(II), qN and qP. The patterns differed mainly in the following respects:

- (1) The Fv/Fm, maximal PSII quantum yield, decreased from 0.72 to 0.68 and from 0.7 to 0.6 after 24 h of HL-stress induction for *H. pluvialis* and *D. salina*, respectively (Figure 3 a). There was a



Table 1 | Pigments composition and their relative abundance

HL stressed cells	<i>H. pluvialis</i>			<i>D. salina</i>		
	0 h	24 h	48 h	0 h	24 h	48 h
Chl b/Chl $\alpha$	0.271 $\pm$ 0.004	0.282 $\pm$ 0	0.273 $\pm$ 0.003	0.363 $\pm$ 0.013	0.352 $\pm$ 0.020	0.318 $\pm$ 0.026
N/Chl $\alpha$	0.115 $\pm$ 0.001	0.110 $\pm$ 0.001	0.113 $\pm$ 0	0.124 $\pm$ 0.005	0.128 $\pm$ 0.012	0.121 $\pm$ 0.001
V/Chl $\alpha$	0.076 $\pm$ 0.001	0.066 $\pm$ 0	0.050 $\pm$ 0	0.123 $\pm$ 0.004	0.082 $\pm$ 0.014	0.044 $\pm$ 0.004
A/Chl $\alpha$	0.004 $\pm$ 0	0.045 $\pm$ 0	0.092 $\pm$ 0	0.006 $\pm$ 0.001	0.080 $\pm$ 0.007	0.096 $\pm$ 0.008
L/Chl $\alpha$	0.446 $\pm$ 0.001	0.487 $\pm$ 0.004	0.548 $\pm$ 0.002	0.26 $\pm$ 0.008	0.382 $\pm$ 0.007	0.467 $\pm$ 0.009
Z/Chl $\alpha$	0 $\pm$ 0	0.025 $\pm$ 0	0.080 $\pm$ 0	0 $\pm$ 0	0.062 $\pm$ 0.006	0.137 $\pm$ 0.008
VAZ/Chl $\alpha$	0.080 $\pm$ 0.001	0.137 $\pm$ 0.001	0.223 $\pm$ 0	0.130 $\pm$ 0.005	0.223 $\pm$ 0.023	0.277 $\pm$ 0.015
AZ/VAZ	0.055 $\pm$ 0.003	0.514 $\pm$ 0	0.774 $\pm$ 0	0.050 $\pm$ 0.004	0.636 $\pm$ 0.026	0.842 $\pm$ 0.015

Chl b, chlorophyll b; Chl  $\alpha$ , chlorophyll  $\alpha$ ; N, neoxanthin; V, violaxanthin; A, antheraxanthin; L, lutein; Z, zeaxanthin; VAZ, the sum of violaxanthin, antheraxanthin and zeaxanthin; AZ, the sum of antheraxanthin and zeaxanthin. Data are mean value of three replicates  $\pm$  SD.

subsequent recovery in *H. pluvialis* at 48 h at a value of 0.75. However, the Fv/Fm of *D. salina* continued to decline to 0.56 at 48 h.

- As shown in Figure 3 b, the ETR(I) of *H. pluvialis* declined by 30% at 24 h and 42% at 48 h. Comparatively, in *D. salina* the ETR(I) declined by 30.05% in the first stage (from 0 h to 24 h) and underwent a significant recovery in the second stage (24 h to 48 h).
- ETR(II) of *H. pluvialis* decreased by 21% and then increased by 20%. In *D. salina*, ETR(II) continuously decreased by 15% and 14% in the first and second stages, respectively (Figure 3 c).
- The ratio of ETR(I) to ETR(II) in *H. pluvialis* continuously decreased through the course of HL stress (Figure 3 d). However, in *D. salina* there was a two-step response pattern, in which the ratio decreased at 24 h and increased significantly ( $P < 0.01$ ) at 48 h.
- Variation of qN in *H. pluvialis* and *D. salina* were quite different during the course HL stress (Figure 3 e). The qN in *H. pluvialis* was firstly decreased at 24 h and increased significantly at 48 h. Comparatively, the qN in *D. salina* was firstly increased at 24 h and decreased at 48 h.
- The qP, which reflects the proportion of opened PSII reaction centers, decreased in both *H. pluvialis* and *D. salina* at 24 h of HL stress (Figure 3 f). At 48 h, *H. pluvialis* recovered to 113.31% while *D. salina* continued to decrease, compared with the value at 24 h.

**Distribution of thylakoid membrane bands.** *H. pluvialis* and *D. salina* shared some similarity to each other with respect to their thylakoid membrane distribution patterns as measured by sucrose density (Figure 4). The purity of the extracted thylakoid membrane proteins was above 80% for both *H. pluvialis* and *D. salina* (87.30% and 84.22% for *H. pluvialis* and *D. salina*, respectively). When no HL stimulation was applied at 0 h, the main intact thylakoid membranes in both *H. pluvialis* and *D. salina* were stacked between the 20% and 50% sucrose layers. While after 24 h HL stimulation, some thylakoid membranes floated on the 20% sucrose layer in both of the stressed cells. At 48 h under HL stress, the thylakoid membranes of *H. pluvialis* were rarely stacked above the 20% layer. Comparatively, in *D. salina* had more thylakoid membranes stacked above the 20% sucrose layer and less were stacked between the 20% and 50% sucrose layers.

**Photosynthetic protein variations.** The relative quantity of photosynthetic proteins, including light-harvesting proteins, reaction center proteins and electron transfer related proteins, changed significantly during the course of HL induction and the acclimation process.

In the first 24 h of HL induction, chlorophyll binding proteins in *H. pluvialis* dramatically increased both in light harvesting complex I (LHCI) and light harvesting complex II (LHCII), followed by a significant decrease at 48 h (Figure 5 a, b). Comparatively, the chlorophyll binding proteins of LHCI in *D. salina* gradually decreased, while the chlorophyll binding proteins of LHCII gradually increased both at 24 h and 48 h.

Protein subunits constituting the cytochrome *b<sub>6</sub>/f* complex, the electron carrier between PSI and PSII, varied greatly during the HL induction process. As shown in Figure 6 a, the cytochrome *f* level in *H. pluvialis* was decreased by 64% after 24 h of HL induction, with a slight recovery to 53% of the original level. However, as for cytochrome *b<sub>6</sub>* (PetB) and the Rieske Fe-S center protein (PetC) in *H. pluvialis*, their levels fell below the instrument detection level at 24 h and 48 h (Figure 6 b, c). Comparatively, proteins related in electron transfer in *D. salina* showed a different pattern. At 24 h, cytochrome *f* (PetA) dropped by 21%, which was followed by a 12% increase at 48 h (Figure 6 a) compared with the level at 0 h. For the levels of cytochrome *b<sub>6</sub>* (PetB) and the Rieske Fe-S center protein (PetC) in *D. salina*, there was a gradual increase both at 24 h and 48 h (Figure 6 b, c).

For PSII reaction center proteins and the core antenna proteins, including CP43 and CP47, a similar pattern of variability was observed in *H. pluvialis*. The proteins, including D1, D2, CP43 and CP47, decreased significantly at 24 h and recovered at 48 h (Figure 7). However, the same proteins in *D. salina* continued to decrease from 24 h to 48 h.

A 33 kDa protein (PsbO) belonging to the oxygen-evolving complex (OEC) in PSII of *H. pluvialis* decreased dramatically and its level fell below the instrument detection sensitivity at 24 h and 48 h (Figure 8). This protein also decreased by 21% at 24 h in *D. salina*. However, there was a significant increase at 48 h, which was 2.4-fold the original level before HL induction. The PsbS protein in *D. salina* gradually increased under HL stress; however, this protein was not detected in *H. pluvialis* at all (Figure 9).

By gathering all PSI and PSII reaction center proteins, their variation patterns under HL were plotted. As shown in Figure 10, the PSI reaction center in *H. pluvialis* gradually increased in size. For the PSII reaction center proteins, *H. pluvialis* suffered a 48.7% reduction (from 65.7% down to 33.8%) at 24 h, followed by a great recovery up to 75.1% at 48 h. However, both the PSI and PSII center sizes in *D. salina* decreased synchronously during the HL stress from 0 to 48 h.

***H. pluvialis* shows a higher conversion rate of carbon into astaxanthin in response to HL.** When subjected to HL stress, photosynthesis-driven carbon fixation was compromised and less inorganic carbon was fixed. As shown in Figure 11 a, total fixed organic carbon significantly decreased by 75% at 24 h of HL and was even lower at 48 h. However, the conversion ratio of fixed carbon into astaxanthin increased with a prolonged HL-treatment

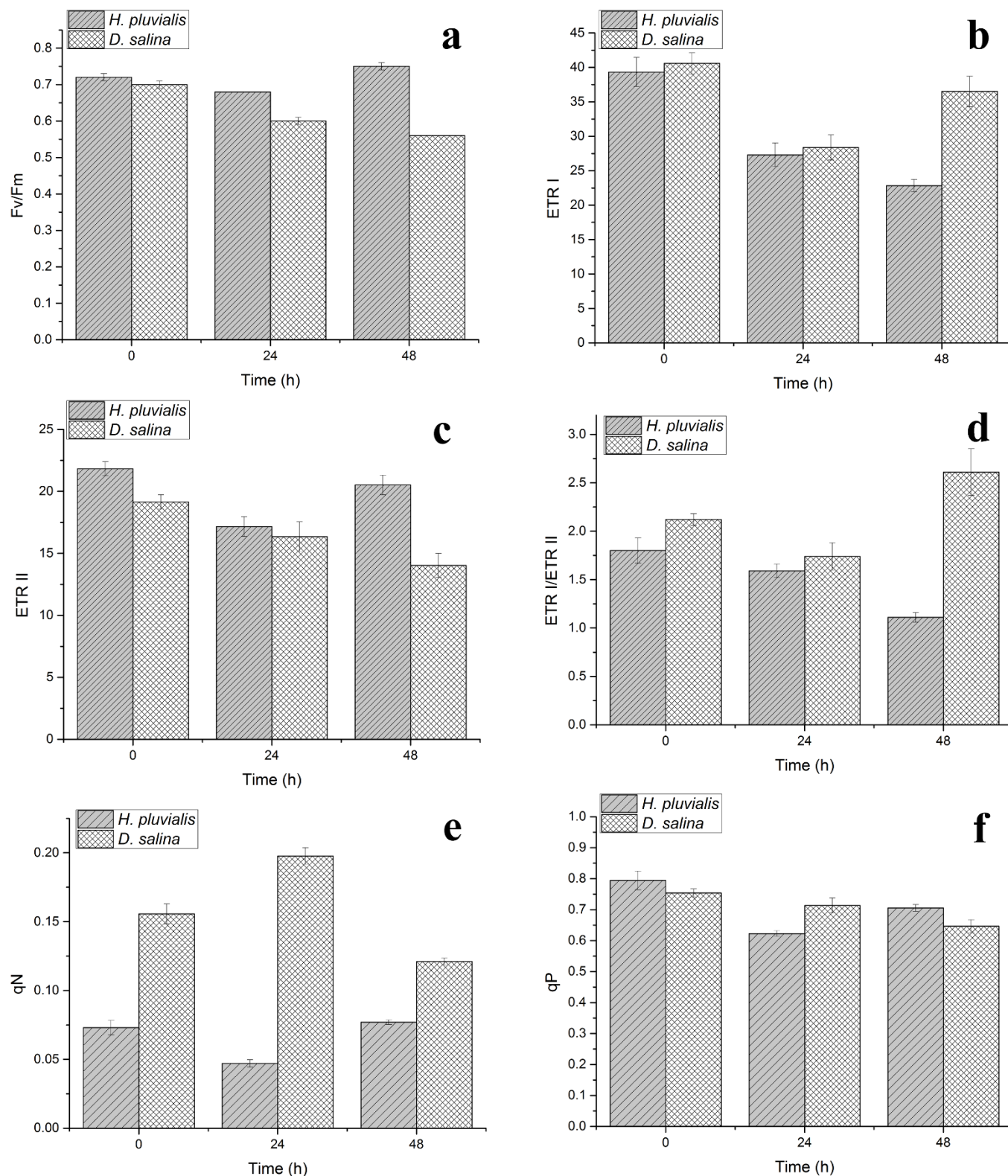


**Figure 3** | PAM analysis of chlorophyll fluorescence in *Haematococcus pluvialis* and *Dunaliella salina* cells: (a), Fv/Fm (maximal PSII quantum yield); (b), ETR(I) (electron transport rate of PSI); (c), ETR(II) (electron transport rate of PSII); (d), Ratio of ETR(I) to ETR(II) in *H. pluvialis* and *D. salina* cells; (e), qN (coefficient of non-photochemical quenching); (f), qP (coefficient of photochemical quenching).

time, with values of 13.77%, 49.62% and 74.02% at 0, 24 and 48 h of HL treatment, respectively (Figure 11 b). Additionally, the carbon anhydrase (CA) activity was also measured. As is shown in Figure 11 c, HL stress decrease CA activity at 24 h by 70.48%. However, CA activity showed a significant increase of 84.42%.

## Discussion

**Thylakoid membrane of *H. pluvialis* might be more extensively protected.** Although HL caused quite similar morphological and growth changes in the two microalgae, for example, the loss of flagella and cell density declines (Figures 1 and 2), thylakoid

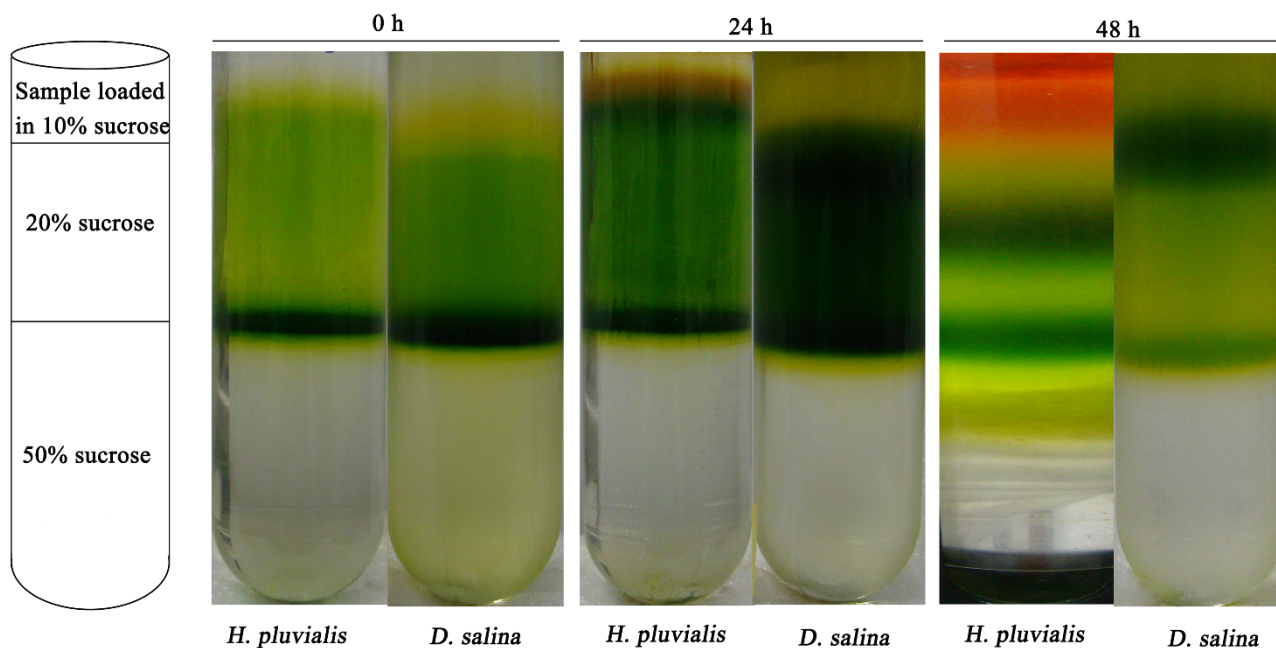


**Figure 4** | Thylakoid membrane distributions in sucrose density solution under high light (HL) stress.

membranes under HL were different in the two algae. The thylakoid membrane was very much vulnerable to HL induced photooxidative damage<sup>12</sup>. Thus, the consequence of HL irradiation on the thylakoid membrane can be fatal and even directly lead to cell death. Before HL induction, the thylakoid membranes of *H. pluvialis* and *D. salina*, which stacked between the 20% and 50% layers in a sucrose gradient, possessed structural integrity and homogeneity (Figure 4). Subsequently, 24 h of HL illumination caused some of the thylakoid fragments to float above the 20% sucrose layer, but still left the main partition between 20% and 50% layers for both cells. This phenomenon revealed that either the fragmentation of the thylakoid membranes, or an increase of lamellae thylakoid was induced by HL<sup>23</sup>, based on the fact that more lamellae could lead to a lower density of the total thylakoid membrane<sup>24</sup>. It has also been reported that HL can lead to the reduction of the appressed thylakoid domain (grana) so that thylakoid lamellae would be relatively increased<sup>25</sup>, resulting in the variation of thylakoid band distribution patterns<sup>24</sup>. As shown (Figure 4), 48 h of HL induction caused a higher percent of low density thylakoids in *D. salina*, but less

in *H. pluvialis*. In *H. pluvialis*, the thylakoid membrane grana structure may have been more extensively protected under HL compared with in *D. salina*. However, HL could lead to the alteration of the fatty acid composition in the membrane, which in turn might affect the density of membrane protein. For example, HL could lead to the increase of saturated fatty acid and decrease of unsaturated fatty acid in *Chlorella vulgaris*<sup>26</sup>.

***H. pluvialis* was more efficient in HL acclimation compared to *D. salina*.** By applying 1,000  $\mu\text{mol photons/m}^2/\text{s}$  irradiance, HL stress was created for both microalgae, which could also be confirmed by the decline of cell density (Figure 2) and Fv/Fm (Figure 3 a). HL stress could lead to higher energy absorbance by LHCII. This resulted in the decrease of vulnerable proteins constituting the PSII complex, including OEC, CP43, CP47, D1 and D2 for both *H. pluvialis* and *D. salina* at 24 h (Figures 7 and 8). Since reaction center proteins were decreased, while the LHCII was relatively increased, at 24 h (Figures 5 and 7), the relatively over-reduced state at PSII needed to be regulated. For photosynthetic organisms, it is critically

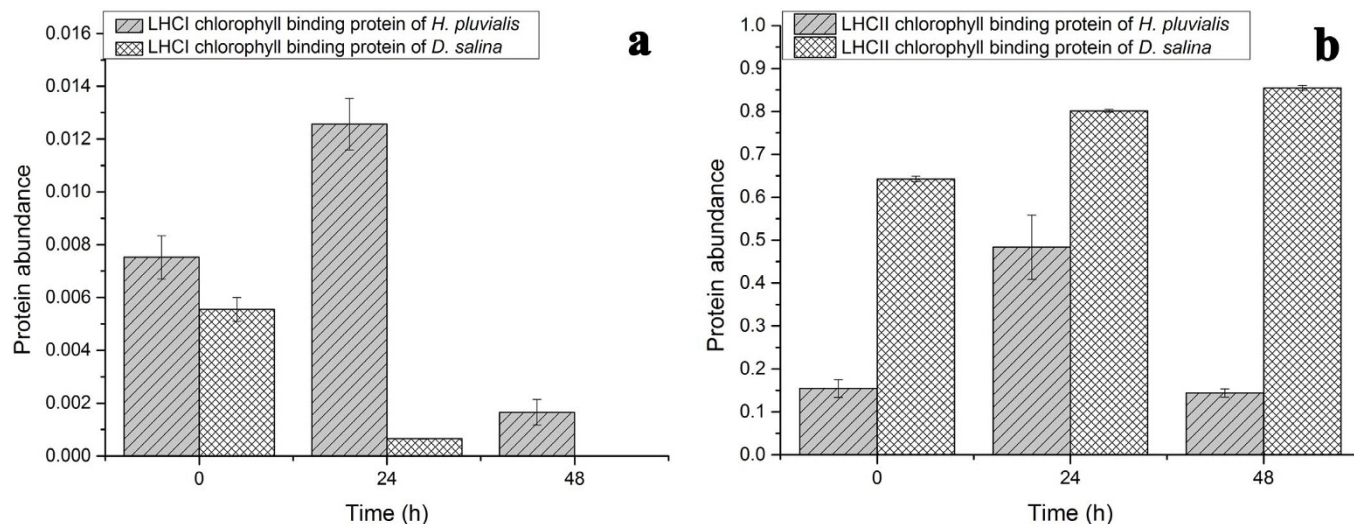


**Figure 5** | Light harvesting complexes (LHC) proteins' abundance variance under high light (HL) stress: (a), LHCI proteins; (b), LHCII proteins.

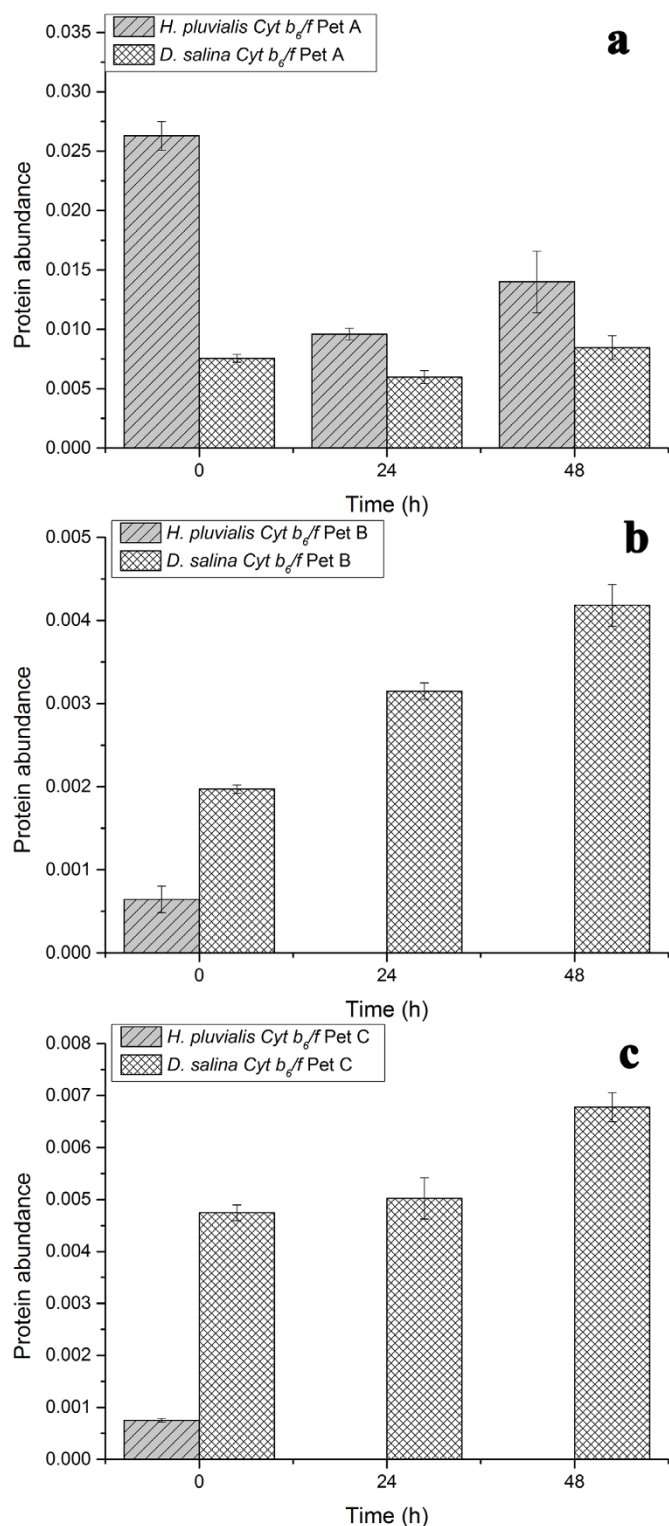


**Figure 6** | Cytochrome  $b_6/f$  complex proteins' abundance variance under high light (HL) stress: (a), Cyt  $b_6/f$ , PetA; (b), Cyt  $b_6/f$ , PetB; (c), Cyt  $b_6/f$ , PetC.

important to maintain a coordinated electron transfer rate so that the redox poise will be stabilized at a balanced state when encountering HL stress<sup>27</sup>. To accomplish this, the ETR(I) and ETR(II) declined (Figure 3 b, c) synchronously for both *H. pluvialis* and *D. salina* at 24 h. The decline of ETR(I) and ETR(II) could be related to the cytochrome  $b_6/f$  complex. Subunits of cytochrome  $b_6/f$  complex work in tandem patterns, thus the decline of any subunit could

lead to inefficient functioning of the photosynthetic electron transport (PET). Consequently, PSI received far less PSII-generated electrons via linear PET for both *H. pluvialis* and *D. salina*. Under such circumstances, PSI activity could be well protected<sup>9</sup>, but PSII would still suffer from an over-reduction.

With HL stress continued at 48 h, *D. salina* increased ETR(I) while ETR(II) was still suppressed (Figure 3 b, c). This stress-responsive strategy is typical and a cyclic PET pathway around PSI was able to funnel excess electrons to generate ATP without increasing oxygen evolution. The widened gap between ETR(I) and ETR(II) enabled a more efficient electron diversion from PSII to PSI, defending PSII from further damage<sup>28</sup>. This responsive mechanism was fully supported by the increase of the electron carrier protein, the cytochrome  $b_6/f$  complex, at 48 h (Figure 6 a). Additionally, the increased PsbS protein in *D. salina* could be involved in PSII protection via feed-back de-excitation (qE), because the overexpression of *PsbS* could increase qE capacity<sup>29</sup>. Nevertheless, *D. salina* did not acclimate well to HL stress, which could be concluded from the persistent decline of  $F_v/F_m$ , qP and the PSI and PSII reaction center proteins (Figures 3 a and 10).

However, *H. pluvialis* seemed to employ another different strategy by narrowing down the gap between ETR(I) and ETR(II) at 48 h, which could be concluded from the declining ratio of ETR(I) to ETR(II) (Figure 3 d). And the strategy turned out to be more effective as  $F_v/F_m$ , PSI and PSII reaction center proteins were recovered at 48 h while those of *D. salina* didn't (Figures 3, 7 and 10). Those facts indicated that there was a different electron diversion mechanism to relieve the over-reduction stress caused by HL in *H. pluvialis*. However, one phenomenon should be noted, that PetB and PetC proteins decreased and fell below the instrument detection sensitivity after 24 h HL stress. Also, the rapid decline of cytochrome  $f$  under HL stress in *H. pluvialis* found in this research (Figure 6 a) was consistent with results by Tan *et al.*<sup>9</sup>. It is known that increased PSI can enhance the cyclic PET pathway to relieve the tension. Yet, the conventional cyclic PET pathway heavily relies on a functional linear PET, involving cytochrome  $b_6/f$ , to transfer PSII-generated electrons. Based on our results, the cytochrome  $b_6/f$  complex was nonfunctional and unable, or at least quite inefficient, to contribute to the linear PET pathway. Consequently, it was highly unlikely that *H. pluvialis* employed a cyclic PET strategy at 48 h. As shown in Figure 3 b, there was still moderate ETR(I) at 48 h, raising the question of the origin of the electrons that drive PSI.

Additionally, the high efficiency of HL acclimation in *H. pluvialis* could be reflected in the recovery of qP at 48 h (Fig. 3 F). The qN parameter also showed a significant increase at 48 h, indicating an efficient ability to dissipate excessive energy. Comparatively, no such phenomenon was observed in *D. salina*. The pool size for the xanthophyll-cycle and conversion ratio were both relatively higher in *D. salina* compared with *H. pluvialis* (Table 1). Yet, the decreasing qN suggested that it might not be sufficient enough for the xanthophyll-cycle alone to cope with HL. Consequently, the higher HL tolerance in *H. pluvialis* could be attributed to more than the xanthophyll-cycle when compared with *D. salina*.

**Decrease of cytochrome  $b_6/f$  was beneficial for astaxanthin synthesis.** HL-induced oxidative stress was directly caused by reactive oxygen species (ROS), including  $H_2O_2$ ,  $O_2^-$ ,  $-OH^*$  and  $^1O_2^{*30}$ , and the chloroplasts were believed to be the primary site of photooxidative damage<sup>16</sup>. Han *et al.* also found that 24 h of HL caused high amounts of ROS accumulation in the motile cells of *H. pluvialis*<sup>16</sup>. The great decline of cytochrome  $b_6/f$  observed in this research and the results by others<sup>9</sup> demonstrated that this could lead to the decrease of the electron transfer from PSII to PSI. The over-excited P680\* could not transfer energy to the photosystem, but to oxygen, forming singlet oxygen ( $^1O_2^{*31}$ ). Although the direct fatal damage of singlet oxygen to *H. pluvialis* cells was unlikely, as has

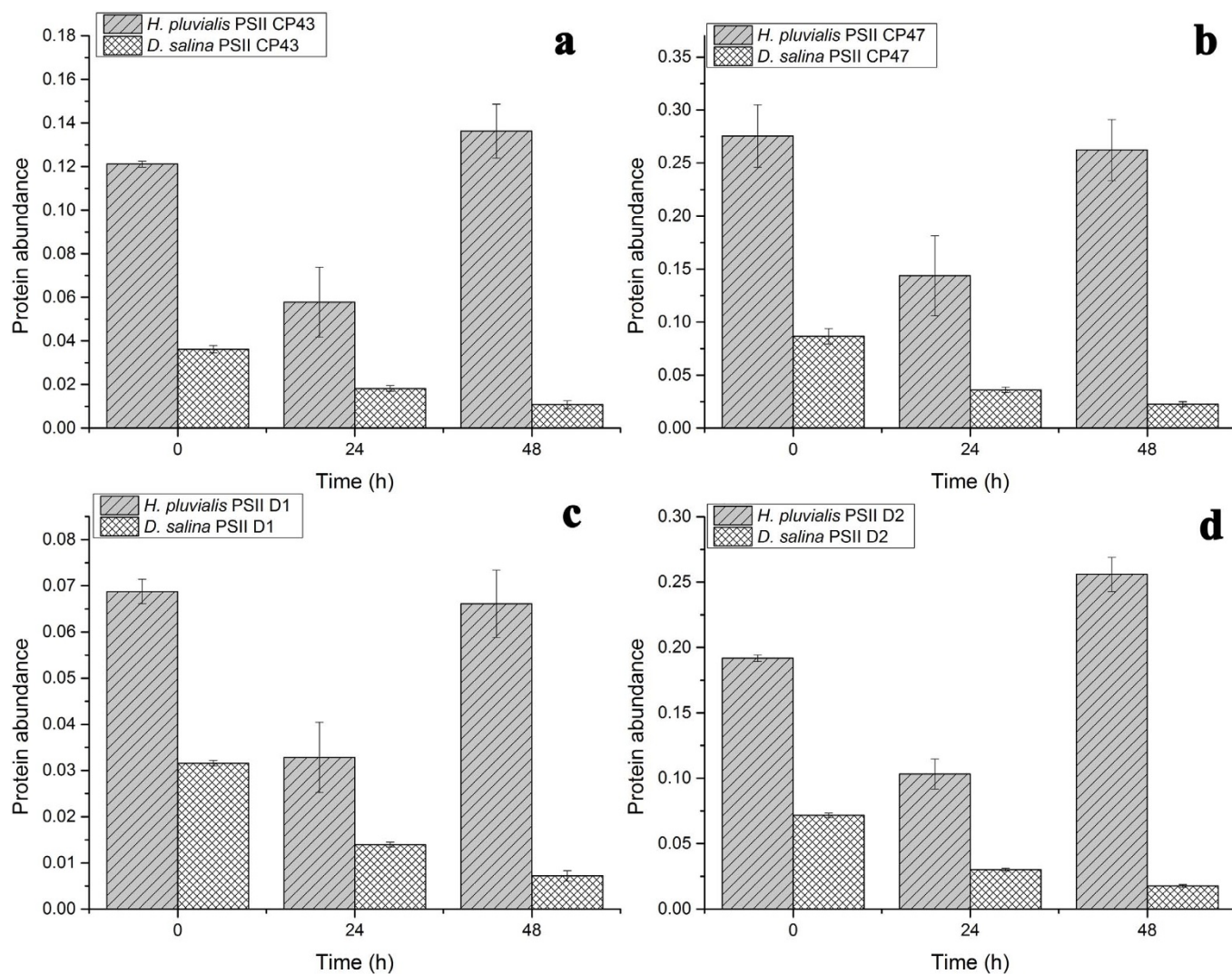


**Figure 7** | Photosystem (PS) II proteins' abundance variance under high light (HL) stress: (a), CP43 protein; (b), CP47 proteins; (c), PSII D1 protein; (d), PSII D2 protein.

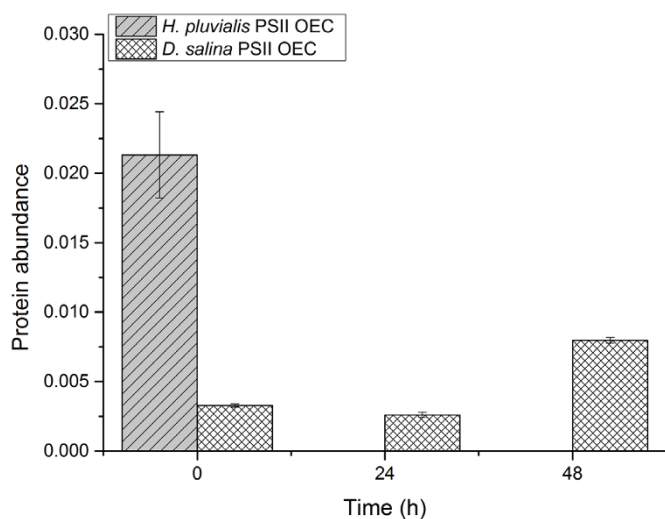


**Figure 8** | Oxygen evolving complex (OEC) protein abundance variance in *Haematococcus pluvialis* and *Dunaliella salina* under high light (HL) stress.

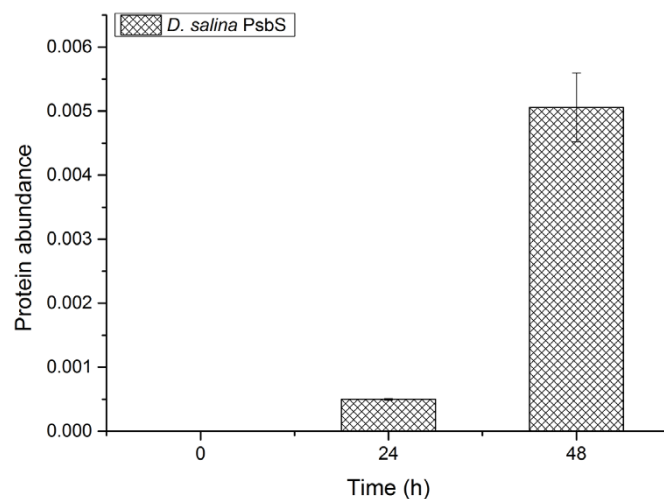


**Figure 9** | PSII S protein (PsbS) protein abundance variance in *Dunaliella salina* thylakoids under high light (HL) stress.

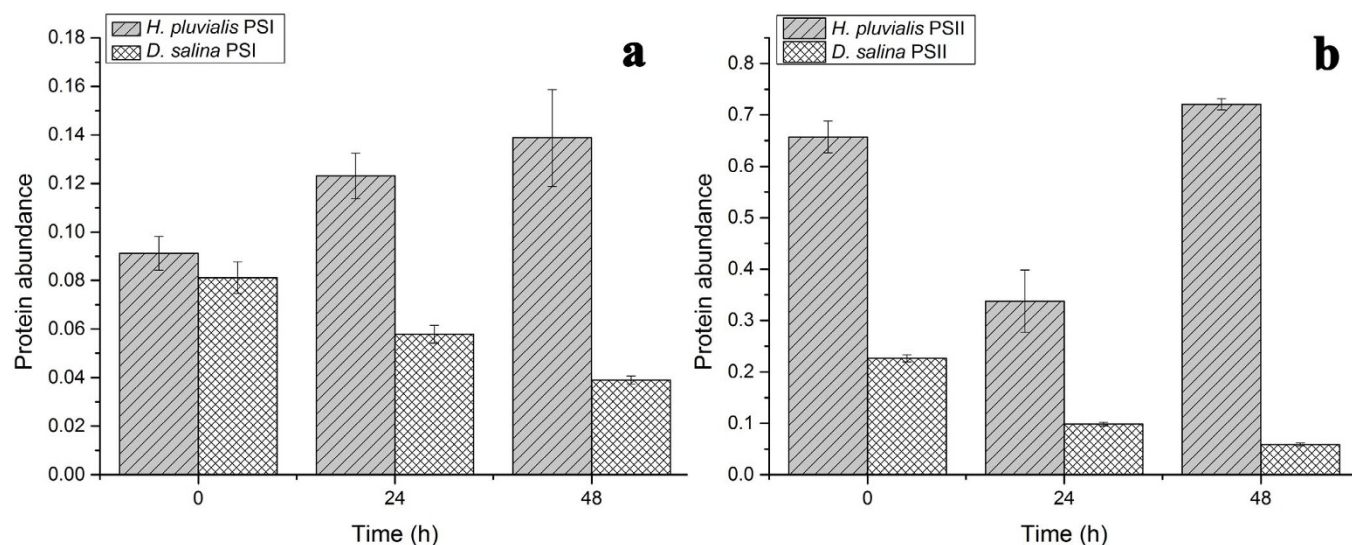


**Figure 10** | PSI and PSII abundance variance in *Haematococcus pluvialis* and *Dunaliella salina* under high light (HL) stress.

been discussed<sup>16</sup>, singlet oxygen was indeed a qualified plastid-generated signal that might be involved in nuclear gene regulation<sup>32</sup>. Yet, how singlet oxygen regulates HL-induced secondary carotenoid synthesis has not been well explained.

The decrease of the cytochrome *b<sub>6</sub>/f* complex also caused an over-reduction of PSI by breaking the cyclic PET around PSI. Meanwhile, there was an increase of LHCI in *H. pluvialis* (Figure 5 a), creating an over-reduction stress for PSI in *H. pluvialis*. Consequently, the generation of superoxide and H<sub>2</sub>O<sub>2</sub> by PSI would be favored<sup>31</sup>. The combined stress caused by both the cytochrome *b<sub>6</sub>/f* decline and the LHCI increase could lead to high amounts of superoxide and H<sub>2</sub>O<sub>2</sub> accumulation. As has been depicted, stressor-dependent carotenogenesis, induced by HL, improved the cell survival rate<sup>12</sup>. ROS accumulation was also due to astaxanthin synthesis requiring more oxygen in the oxidation and hydroxylation steps when compared with  $\beta$ -carotene synthesis<sup>8</sup>. Those oxygen-consuming reactions would remove the excess intracellular oxygen produced during ROS detoxification. Overall, while the cytochrome *b<sub>6</sub>/f* complex decline might appear to negatively affect photosynthesis, it was actually an early preparation for astaxanthin synthesis during long-term acclimation.

#### Differences between *H. pluvialis* and *D. salina* in response to HL.

For both *H. pluvialis* and *D. salina*, normal light provides moderated levels of irradiation energy to drive photosynthesis, thus the linear PET dominated, generating ATP and NADPH. Such a conventional PET pattern provided sufficient reduction power to fuel the Calvin cycle for carbon fixation, as depicted in Figure 12. Under such circumstance, cell proliferation metabolism would be favored and biomass was accumulated. However, *H. pluvialis* showed a dramatic decline in the cell proliferation rate and increase of cyst cells under HL stress<sup>33</sup>. Secondary carotenoid accumulation occurred in cyst cells under unfavorable environments, including HL, nutrient deprivation, salt stress and oxidative stress<sup>34,35</sup>. Mostly, astaxanthin accumulation was accompanied cell enlargement<sup>14</sup> and adding carbon sources, like acetate, CO<sub>2</sub> or NaHCO<sub>3</sub> enhanced the astaxanthin accumulation<sup>36</sup>. Although the photosynthetic activity was compromised under stress in *H. pluvialis*, the carbon source was still assimilated, and Hagen *et al.* believed stressed cells store carbon and energy for recovery after stress<sup>37</sup>.

When encountering HL stress, although many physiological and photosynthetic proteome differences existed between *H. pluvialis* and *D. salina*, there was a common purpose of cellular survival. For *D. salina*, the increased cytochrome *b<sub>6</sub>/f* complex could help

transfer PSII generated electrons and increase cyclic PET around PSI while producing ATP under HL. For *H. pluvialis*, the great decline in the cytochrome *b<sub>6</sub>/f* complex broke the linear PET, thus the reduction power (NADPH) and ATP production were restrained. In fact, *H. pluvialis* was able to accumulate astaxanthin, starch and oil globules under HL<sup>9,16</sup>, and in those cases the reduction power, ATP and carbon material (i.e. acetyl-CoA) were all heavily required. Many widely accepted theories have been established to explain the HL-responsive mechanism in *H. pluvialis*<sup>8,10,11,16</sup>. A dominant one is that *H. pluvialis* and other higher plants employ a plastid terminal oxidase (PTOX)-involved mechanism to regulate the internal redox poise under HL stress<sup>15,16,28,38,39</sup>. However, a conventional carbon assimilation process would not be driven efficiently due to the decreased cytochrome *b<sub>6</sub>/f* complex. Consequently, *H. pluvialis* needs to balance the reduction power and to make the most of the carbon source available. *H. pluvialis* must manage HL stress while fuelling a carbon sink at the same time.

Based on our results and previous research, we propose a possible systematic metabolic network that covers both photosynthetic acclimation and carbon flow reorientation (Figure 12). For *H. pluvialis*, the reduction power could be provided by the photosynthesis process and cellular metabolism. Due to the partially destroyed PET pathway, less reduction power was generated by regular photosynthesis. Thus, other complementary pathways would be required for first starch, and subsequent astaxanthin and fatty acid synthesis. Wang *et al.* reported the up-regulation of proteins involved in glycolysis and the pentose phosphate pathway under oxidative stress<sup>11</sup>. Results by Chen *et al.*<sup>40</sup> showed that astaxanthin synthesis was accompanied by significant up-regulation of both Rubisco activity and *rbcl* gene expression, indicating possible Rubisco participation in astaxanthin synthesis. However, it seemed unnecessary to maintain a high Rubisco activity while photosynthesis was compromised by HL, unable to provide sufficient reduction power for carbon fixation. The reduction power requirement constraint could break the Calvin cycle by suspending the regeneration of RuBp. In fact, it has been reported that Rubisco could participate in metabolite conversion without the Calvin cycle<sup>41</sup>, in which case the RuBp requirement by Rubisco could be fulfilled by the pentose phosphate pathway.

Photosynthetic proteome results and previous conclusions suggested it is both necessary and possible that a reoriented carbon flow pathway exists in *H. pluvialis* under HL. Under HL stress, conventional linear PET was greatly compromised due to a decrease in the cytochrome *b<sub>6</sub>/f* complex. Insufficient reduction power would not be able to drive the Calvin cycle. However, the pentose phosphate path-



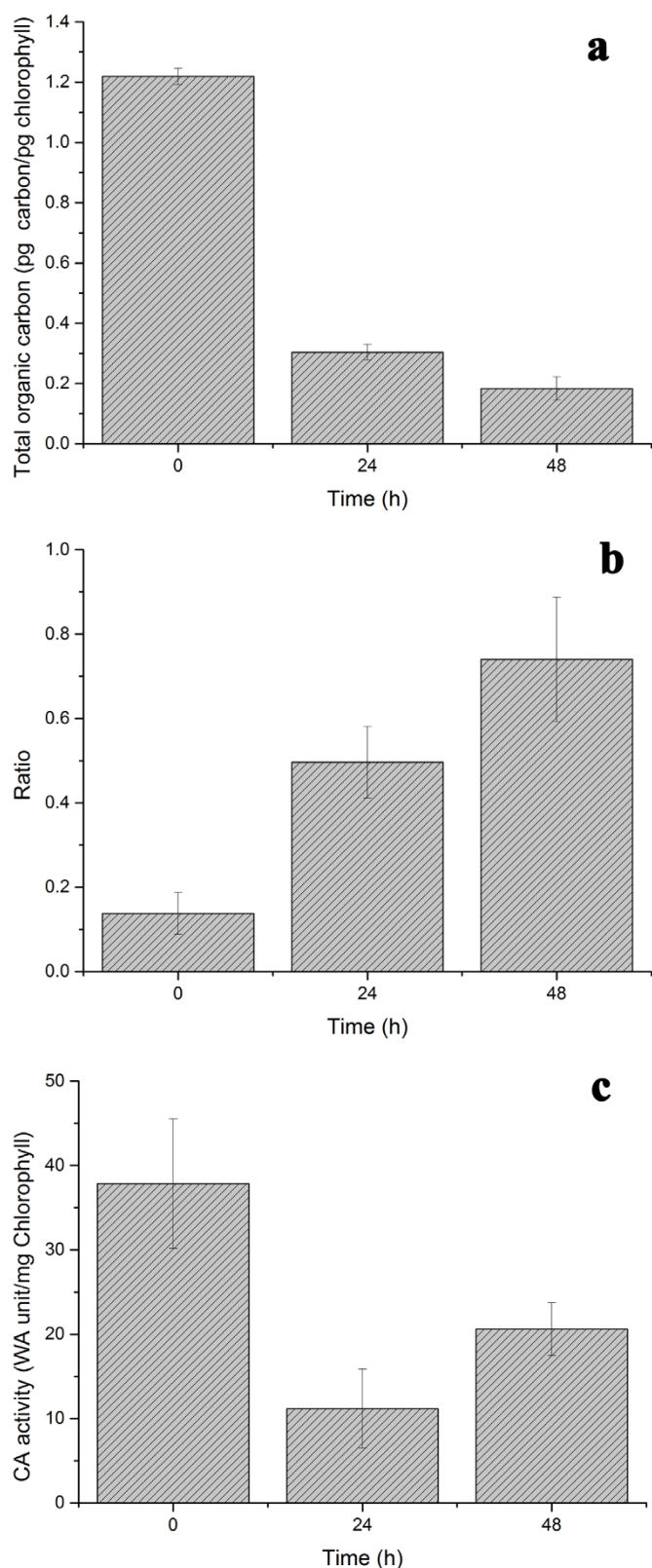


**Figure 11 | Carbon fixation, astaxanthin conversion variation and CA enzyme activity in *Haematococcus pluvialis*.** (a), total organic carbon fixed at different high light (HL) stress stages. (b), the ratio of astaxanthin conversion from fixed organic carbon; (c), CA (carbon anhydrase) enzyme activity.

way diverted RuBp to the Calvin cycle to maintain the carbon fixation process. The 3-phosphoglycerate (3PGA) produced from the fixation step of the Calvin cycle would be mostly diverted to glycolysis for acetyl-CoA production to meet the great demand for carbon skeleton buildup during fatty acid and carotenoid synthesis. The shared tank of ATP and reduction power during carbon sink construction can also be complementarily fuelled by the TCA cycle. Overall, it is an economic and effective pathway for carbon assimilation when photosynthesis is inhibited by HL. It has been experimentally verified that carbon sources, like  $\text{HCO}_3^-$  or  $\text{CO}_2$ , and acetate enhanced astaxanthin accumulation<sup>34,42</sup>. Consequently, it is theoretically possible for *H. pluvialis* to quickly form intracellular carbon sinks with minimized restrictions caused by the photosynthetic decline, even though the hypothesis requires experimental verification.

**The maintenance of increased efficiency of carbon incorporation in *H. pluvialis*.** As proposed in Figure 12, the occurrence of carbon sink formation, mainly through astaxanthin synthesis, was possible, and the enlargement of cell diameters (Figure 1) suggested that extracellular inorganic carbon were required. By using isotope-labelled inorganic carbon, the inorganic carbon-fixation capability was measured under HL stress. The decrease in fixed organic carbon (Figure 11 a) confirmed the negative influence by HL stress. However, the increased conversion ratio to astaxanthin (Figure 11 b) implied that a carbon flow reorientation occurred under HL in *H. pluvialis*. The carbon flow regulation could also be reflected by the increase of CA activity at 48 h of HL. Although total fixed carbon dropped at 48 h compared with the level at 24 h, CA activity was increased at 48 h. Moreover, the elevated astaxanthin conversion ratio and the increase of CA activity were more than just coincidental occurrences at 48 h of HL. In fact, the increase of CA activity should be considered a prerequisite for the rapid carbon sink formation under HL.

Additionally, there remained another unknown mechanism that regulated the distribution of carbon flux fuelled into the carbon sink of starch, astaxanthin and fatty acids. It has been reported that pyruvate kinase was down-regulated under oxidative stress<sup>11</sup>. In the proposed metabolic pathway, whether pyruvate kinase played a control role in carbon flux distribution remains to be verified.

## Methods

**Algae and cultivation.** *H. pluvialis* Flotow and *D. salina* were conserved in our laboratory. *H. pluvialis* was cultured in MCM medium<sup>43</sup> at  $22 \pm 1^\circ\text{C}$  with a 12 h light/dark cycle. Light provided by the fluorescent lamps was controlled at  $100 \mu\text{mol photons/m}^2/\text{s}^2$ . Sterilized bubbles of air containing 430 ppm (monitored using a Telaire 7001  $\text{CO}_2$  analyzer, USA) of  $\text{CO}_2$  were continuously aerated into the culture. *D. salina* was cultured in f/2 medium under the same condition as *H. pluvialis*. All samples were cultured in 500-mL Erlenmeyer flasks. Cell growth was monitored using a hemocytometer under a microscope. At the steady plateau stage, cells were subjected to an HL stress of  $1,000 \mu\text{mol photons/m}^2/\text{s}$  for 24 h and 48 h. To eliminate cell rhythm effects, cells under HL stress continued to be cultivated under a 12-h light/dark cycle.

**Chlorophyll fluorescence measurements.** For the chlorophyll fluorescence analysis, a computer-controlled chlorophyll fluorometer, Dual-PAM-100 (Heinz Walz GmbH, Germany), was used. The amount of algal sample used per fluorescence measurement was adjusted according to a total chlorophyll content of 1 mg/mL. Samples were dark-adapted for 15 min before measurement. Both the relative rates of electron transport via photosystem I (PSI) and photosystem II (PSII), known as ETR(I) and ETR(II), respectively, were calculated based on the data acquired during induction curve measurement. During the induction curve measurement, the artic light was set at  $95 \mu\text{mol photons/m}^2/\text{s}^2$ . A saturation pulse light of 635 nm ( $10,000 \mu\text{mol photons/m}^2/\text{s}^2$  intensity, 300 ms duration) was used. The  $q_N$ , coefficient of nonphotochemical quenching, was calculated using  $q_N = (F_m - F_m') / (F_m' - F_0')$ , in which  $F_m$  and  $F_m'$  were maximal fluorescence yield values measured in dark-adapted and light-adapted samples, respectively.  $F_0'$  was the minimal fluorescence yield of illuminated sample. The  $q_P$ , coefficient of photochemical quenching, was calculated as described by Maxwell *et al.*<sup>44</sup>. Four independent biological replicates were measured for each group.

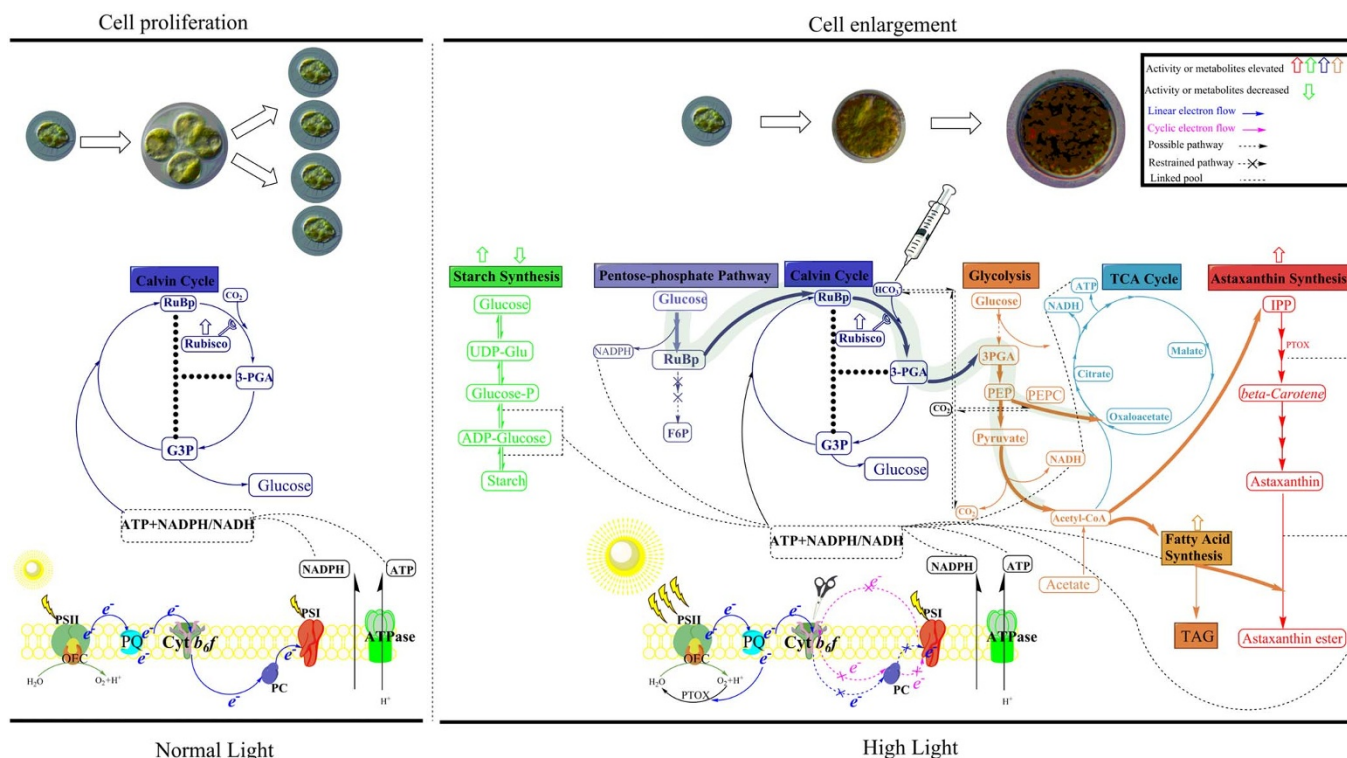


**Figure 12** | A schematic diagram depicting *Haematococcus pluvialis* metabolic pathways under normal light and high light (HL). The light-blue pathway in the background indicates the carbon flow direction under HL stress.

**Thylakoid membrane isolation.** Thylakoid membranes were isolated as described<sup>10</sup> with minor modifications. Briefly, approximately 4 g (fresh weight) of cell pellet was suspended in 40 mL of pre-cooled (4°C) extraction buffer (10% sucrose, 25 mM HEPES-KOH, 1 mM MgCl<sub>2</sub> and 0.1 mM ε-amino caproic acid; pH 7.5). Discontinuous sucrose gradient (20% and 50% sucrose, w/v) ultracentrifugation at 105,000 g for 4 h at 4°C (Beckman Coulter Optima L-100K, SW40 Ti rotor, USA) was applied for thylakoid purification. The green bands between sucrose gradient layers (between 10% and 20%, and between 20% and 50%) were collected. To remove sucrose from the thylakoid membrane sample, the collected sample was diluted with 10 volumes of stock buffer (5 mM HEPES-KOH, 10 mM EDTA and 0.1 mM ε-amino caproic acid; pH 7.5) and ultracentrifuged at 105,000 g for 1 h at 4°C (Beckman Coulter Optima L-100K, SW32 Ti rotor, USA). The thylakoid membrane pellet was stored at -80°C for further analysis. To preserve the integrity of the thylakoid membrane and prevent protein degradation, all procedures of thylakoid membrane isolation and purification were carried out under dim light at a low temperature (0°C), except when specified.

**Photosynthetic pigments analysis.** Pigments were extracted using a solvent containing acetone/methanol (v : v = 1 : 1) and analyzed using a ZORBAX reverse-phase C18 column with HPLC (Agilent 1200, USA) as described<sup>10</sup>. Signals of different pigments were normalized to the peak area of chlorophyll *a*. Pigments were identified on the basis of absorption spectra and the retention time of the pigment's standards. Three independent samples were extracted and measured.

**Protein extraction and desalting.** Thylakoid membrane proteins were precipitated using 10% (w/v) TCA in cold acetone to remove adhered pigments. Denatured protein was solubilized in 8 M urea in 125 mM NH<sub>4</sub>HCO<sub>3</sub>. Subsequently, protein desalting was conducted by fast ultrafiltration using an Amicon Ultra 3K device (Millipore, Ireland).

**Protein determination and trypsin digestion.** Concentrations of desalted protein samples were determined as described<sup>45</sup> using bovine serum albumin as the standard. Proteins solubilized in 100 μL of 8 M urea were reduced in 10 mM DTT (at 56°C, 1 h) and alkylated in the dark with 50 mM iodoacetamide (at 20°C, 1 h) before tryptic digestion. To preserve trypsin activity, the urea concentration was diluted to 1 M by adding 700 μL of 125 mM NH<sub>4</sub>HCO<sub>3</sub>. The protein in-solution digestion was conducted by adding 1/30 (w/w) sequencing grade modified trypsin (Promega, USA) followed by 12 h in a 37°C water bath. Formic acid was added to a final concentration of 1% (v/v) to terminate the tryptic digestion process.

**Protein quantitation by a HPLC-QTOF mass spectrometer.** Digested peptides were loaded in a reverse phase HPLC-QTOF mass spectrometer. Peptides were eluted using gradient mobile phase solutions A (0.1% formic acid in distilled water) and B

(0.1% formic acid in acetonitrile) as described previously, with minor modifications<sup>46</sup>. An acetonitrile gradient (5% B for 5 min, linear gradient from 5% to -50% B for 115 min, followed by 95% B for 30 min) was used to elute the peptides at a flow rate of 0.15 mL/min into the Agilent 6520b Q-TOF mass spectrometer. An electrospray voltage of 3.5 kV was used with the drying gas temperature set at 350°C for a dual ESI source. Data acquisition was carried out in the auto MS-MS mode with MassHunter software (version B03.01, Agilent, USA). Three replicates were processed independently.

**Data processing for protein identification and quantitative analysis.** MS-MS spectra were processed using the Spectrum Mill MS Proteomics Workbench (version A.03.03, Agilent) and filtered MS-MS spectra data were searched against the NCBI database (retrieved on 26 April 2013) for protein identification. Precursor mass tolerance was set at ±20 ppm. One missed cleavage site was allowed in sequence matches. All protein identifications with a protein score ≥ 25 and a peptide SPI ≥ 60%, or a protein score ≥ 15 with no less than two unique peptides identified, were considered as positive identifications. Total peptide ion intensities corresponding to each protein were used for relative protein quantification. Protein abundance was normalized by global intensity using equation (1) as described by Griffin *et al.*<sup>47</sup>. Additionally, the thylakoid membrane protein purity test, based on the above mentioned protein quantification method, was also conducted.

$$SI_{GI} = SI / \sum_{j=1}^n SI_j \quad (1)$$

where,

SI<sub>GI</sub> is protein abundance normalized to global intensity

SI is protein abundance

SI<sub>j</sub> is abundance of the *j*th protein

*n* is the number of identified proteins

**Carbon anhydrase activity measurement.** The extracellular carbon anhydrase activity was measured using the potentiometric method as described previously<sup>48</sup>. Briefly, cells were suspended in sodium barbital buffer (20 mM, pH 8.3) and subjected to CO<sub>2</sub>-saturated distilled water at 0°C. The time required for the pH to drop from 8.3 to 7.0 was recorded. Carbon anhydrase was standardized to total chlorophyll and calculated in Wilbur-Anderson units (WA units) as described<sup>48</sup>. The total chlorophyll content was extracted and determined as described<sup>10</sup>.

**Isotope labeling and quantitation.** The cell cultures were dark adapted for 1 h before isotope labeling. Then, 50 μL of NaH<sup>14</sup>CO<sub>3</sub> (0.2 μCi, ICN Radiochemicals, England), together with 0.05 M NaHCO<sub>3</sub>, was added as the inorganic carbon source. The cultures were subsequently transferred to silica vessels for incubation at low and HL, respectively, for 48 h. Cells were filtered on to glass fiber membranes (Whatman,



England) and incubated with concentrated HCl to remove the unfixed inorganic carbon. Astaxanthin extraction and separation was performed as previously described<sup>8</sup>. Dissolved inorganic carbon (DIC) was determined using a Total Organic Analyzer (Shimadzu TOC-5000 A, Japan). The total isotope content in organic carbon and astaxanthin was measured using a scintillation counter (Beckman LS6500, USA). Three biological replicates were measured. Total carbon fixation was calculated using the following equation as described by Nielsen<sup>49</sup>:

$$\mu\text{g carbon/L} = \frac{(CPM_L - CPM_D) \times If \times DIC}{Ce \times A}$$

where,

$CPM_L$  is the number of counts per minute in the experimental group,  
 $CPM_D$  is the number of counts per minute in the dark comparison group, and  
 $If$  is the isotope discrimination factor. During the fixation of  $CO_2$ , the fixation efficiency of  $^{13}C$  is higher than  $^{14}C$  by 6%, thus  $If$  value is 1.06.

$DIC$  is the dissolved inorganic carbon,  
 $Ce$  is the counting efficiency, which was obtained by measuring standard  $^{14}C$  samples, and  
 $A$  is the number of  $\mu Ci$  multiplied by  $2.2 \times 10^6$ .

**Data and statistical analysis.** All statistical data analysis was conducted by SAS 9.1 for Windows software (SAS Institute Inc., USA). One-way analysis of variance was used to determine the significant difference at  $P < 0.05$ . Schematic diagram depicting metabolic pathway was prepared using ChemBioDraw Ultra (Version 14.0, PerKElmer, USA).

- Spetea, C., Rintamäki, E. & Schoefs, B. Changing the light environment: chloroplast signalling and response mechanisms. *Philosophical Transactions of the Royal Society B: Biological Sciences* **369**, 20130220 (2014).
- Kawahara, M. *et al.* Chloroplast avoidance movement reduces photodamage in plants. *Nature* **420**, 829–832 (2002).
- Jiang, C.-D., Gao, H.-Y., Zou, Q., Jiang, G.-M. & Li, L.-H. Leaf orientation, photorespiration and xanthophyll cycle protect young soybean leaves against high irradiance in field. *Environ. Exp. Bot.* **55**, 87–96 (2006).
- Pastenes, C., Pimentel, P. & Lillo, J. Leaf movements and photoinhibition in relation to water stress in field-grown beans. *J. Exp. Bot.* **56**, 425–433 (2005).
- Niyogi, K. K. Photoprotection revisited: genetic and molecular approaches. *Annu. Rev. Plant Physiol. Plant Mol. Biol.* **50**, 333–359 (1999).
- Pascal, A. A. *et al.* Molecular basis of photoprotection and control of photosynthetic light-harvesting. *Nature* **436**, 134–137 (2005).
- Ebenhöh, O., Fucile, G., Finazzi, G., Rochaix, J. D. & Goldschmidt-Clermont, M. Short-term acclimation of the photosynthetic electron transfer chain to changing light: a mathematical model. *Philos Trans R Soc Lond B Biol Sci* **369**, 20130223 (2014).
- Lemoine, Y. & Schoefs, B. Secondary ketocarotenoid astaxanthin biosynthesis in algae: a multifunctional response to stress. *Photosynthesis Res.* **106**, 155–177 (2010).
- Tan, S. *et al.* Cytochrome f loss in astaxanthin-accumulating red cells of *Haematococcus pluvialis* (Chlorophyceae): Comparison of photosynthetic activity, photosynthetic enzymes, and thylakoid membrane polypeptides in red and green cells. *J. Phycol.* **31**, 897–905 (1995).
- Gu, W. *et al.* Comparison of different cells of *Haematococcus pluvialis* reveals an extensive acclimation mechanism during its aging process: From a perspective of photosynthesis. *PLoS One* **8**, e67028 (2013).
- Wang, S.-B., Chen, F., Sommerfeld, M. & Hu, Q. Proteomic analysis of molecular response to oxidative stress by the green alga *Haematococcus pluvialis* (Chlorophyceae). *Planta* **220**, 17–29 (2004).
- Li, Y., Sommerfeld, M., Chen, F. & Hu, Q. Consumption of oxygen by astaxanthin biosynthesis: a protective mechanism against oxidative stress in *Haematococcus pluvialis* (Chlorophyceae). *J. Plant Physiol* **165**, 1783–1797 (2008).
- Wang, B., Zarka, A., Trebst, A. & Boussiba, S. Astaxanthin accumulation in *Haematococcus pluvialis* (Chlorophyceae) as an active photoprotective process under high irradiance. *J. Phycol.* **39**, 1116–1124 (2003).
- Boussiba, S. Carotenogenesis in the green alga *Haematococcus pluvialis*: Cellular physiology and stress response. *Physiol. Plant.* **108**, 111–117 (2000).
- Li, Y., Sommerfeld, M., Chen, F. & Hu, Q. Effect of photon flux densities on regulation of carotenogenesis and cell viability of *Haematococcus pluvialis* (Chlorophyceae). *J. Appl. Phycol.* **22**, 253–263 (2010).
- Han, D. X., Wang, J. F., Sommerfeld, M. & Hu, Q. Susceptibility and protective mechanisms of motile and non motile cells of *Haematococcus pluvialis* (Chlorophyceae) to photooxidative stress. *J. Phycol.* **48**, 693–705 (2012).
- Schoefs, B., Rmiki, N.-E., Rachadi, J. & Lemoine, Y. Astaxanthin accumulation in *Haematococcus* requires a cytochrome P450 hydroxylase and an active synthesis of fatty acids. *FEBS Lett.* **500**, 125–128 (2001).
- Lamers, P. P. *et al.* Carotenoid and fatty acid metabolism in light-stressed *Dunaliella salina*. *Biotechnol. Bioeng.* **106**, 638–648 (2010).
- Nakada, T., Misawa, K. & Nozaki, H. Molecular systematics of Volvocales (Chlorophyceae, Chlorophyta) based on exhaustive 18S rRNA phylogenetic analyses. *Mol. Phylog. Evol.* **48**, 281–291 (2008).
- Helbig, A. O., Heck, A. J. R. & Slijper, M. Exploring the membrane proteome—Challenges and analytical strategies. *Journal of Proteomics* **73**, 868–878 (2010).
- Lello, Z., Anna, M. T. & Christian, G. H. Thylakoid Membrane Proteome: Separation by HPLC and Identification by Accurate Molecular Mass Determinations. *Curr. Proteomics* **1**, 247–260 (2004).
- Neilson, K. A. *et al.* Less label, more free: Approaches in label-free quantitative mass spectrometry. *Proteomics* **11**, 535–553 (2011).
- Stefansson, H., Andreasson, E., Weibull, C. & Albertsson, P.-Å. Fractionation of the thylakoid membrane from *Dunaliella salina* – heterogeneity is found in Photosystem I over a broad range of growth irradiance. *Biochimica et Biophysica Acta (BBA) - Bioenergetics* **1320**, 235–246 (1997).
- Tanaka, A. & Melis, A. Irradiance-Dependent Changes in the Size and Composition of the Chlorophyll a-b Light-Harvesting Complex in the Green Alga *Dunaliella salina*. *Plant and Cell Physiology* **38**, 17–24 (1997).
- Vasilikiotis, C. & Melis, A. The role of chloroplast-encoded protein biosynthesis on the rate of D1 protein degradation in *Dunaliella salina*. *Photosynthesis Res.* **45**, 147–155 (1995).
- Seyfabadi, J., Ramezani, Z. & Amini Khoeyi, Z. Protein, fatty acid, and pigment content of *Chlorella vulgaris* under different light regimes. *J. Appl. Phycol.* **23**, 1–6 (2010).
- Kargul, J. & Barber, J. Photosynthetic acclimation: Structural reorganisation of light harvesting antenna – role of redox-dependent phosphorylation of major and minor chlorophyll a/b binding proteins. *FEBS J.* **275**, 1056–1068 (2008).
- Rumeau, D., Peltier, G. & Cournac, L. Chlororespiration and cyclic electron flow around PSI during photosynthesis and plant stress response. *Plant, Cell Environ.* **30**, 1041–1051 (2007).
- Li, X.-P., Müller-Moulé, P., Gilmore, A. M. & Niyogi, K. K. PsbS-dependent enhancement of feedback de-excitation protects photosystem II from photoinhibition. *Proceedings of the National Academy of Sciences* **99**, 15222–15227 (2002).
- Li, Z., Wakao, S., Fischer, B. B. & Niyogi, K. K. Sensing and responding to excess light. *Annu Rev Plant Biol* **60**, 239–260 (2009).
- Apel, K. & Hirt, H. Reactive oxygen species: Metabolism, Oxidative Stress, and Signal Transduction. *Annu. Rev. Plant Biol.* **55**, 373–399 (2004).
- Beck, C. F. Signaling pathways from the chloroplast to the nucleus. *Planta* **222**, 743–756 (2005).
- Hagen, C., Grünwald, K., Schmidt, S. & Müller, J. Accumulation of secondary carotenoids in flagellates of *Haematococcus pluvialis* (Chlorophyta) is accompanied by an increase in per unit chlorophyll productivity of photosynthesis. *Eur. J. Phycol.* **35**, 75–82 (2000).
- Kobayashi, M., Kakizono, T. & Nagai, S. Enhanced carotenoid biosynthesis by oxidative stress in acetate-induced cyst cells of a green unicellular alga, *Haematococcus pluvialis*. *Appl. Environ. Microbiol.* **59**, 867 (1993).
- Kobayashi, M., Kurimura, Y. & Tsuji, Y. Light-independent, astaxanthin production by the green microalga *Haematococcus pluvialis* under salt stress. *Biotechnol. Lett.* **19**, 507–509 (1997).
- Orosa, M., Franqueira, D., Cid, A. & Abalde, J. Carotenoid accumulation in *Haematococcus pluvialis* in mixotrophic growth. *Biotechnol. Lett.* **23**, 373–378 (2001).
- Hagen, C., Braune, W., Birckner, E. & Nuske, J. Functional aspects of secondary carotenoids in *Haematococcus lacustris* (Girod) Rostafinski (Volvocales) I. The accumulation period as an active metabolic process. *New Phytol.* **125**, 625–633 (1993).
- Ivanov, A. G. *et al.* Implications of alternative electron sinks in increased resistance of PSII and PSI photochemistry to high light stress in cold-acclimated *Arabidopsis thaliana*. *Photosynthesis Res.* **113**, 191–206 (2012).
- Wang, J., Sommerfeld, M. & Hu, Q. Occurrence and environmental stress responses of two plastid terminal oxidases in *Haematococcus pluvialis* (Chlorophyceae). *Planta* **230**, 191–203 (2009).
- Chen, Z., Wang, G. & Niu, J. Variation in Rubisco and other photosynthetic parameters in the life cycle of *Haematococcus pluvialis*. *Chin. J. Oceanol. Limnol.* **30**, 136–145 (2012).
- Schwender, J., Goffman, F., Ohlrogge, J. B. & Shachar-Hill, Y. Rubisco without the Calvin cycle improves the carbon efficiency of developing green seeds. *Nature* **432**, 779–782 (2004).
- Kang, C., Lee, J., Park, T. & Sim, S. Comparison of heterotrophic and photoautotrophic induction on astaxanthin production by *Haematococcus pluvialis*. *Appl. Microbiol. Biotechnol.* **68**, 237–241 (2005).
- Borowitzka, M. A., Huisman, J. M. & Osborn, A. Culture of the astaxanthin-producing green alga *Haematococcus pluvialis* 1. Effects of nutrients on growth and cell type. *J. Appl. Phycol.* **3**, 295–304 (1991).
- Maxwell, K. & Johnson, G. N. Chlorophyll fluorescence—a practical guide. *J. Exp. Bot.* **51**, 659–668 (2000).
- Bradford, M. M. A rapid and sensitive method for the quantitation of microgram quantities of protein utilizing the principle of protein-dye binding. *Anal. Biochem.* **72**, 248–254 (1976).
- Blonder, J., Chan, K. C., Issaq, H. J. & Veenstra, T. D. Identification of membrane proteins from mammalian cell/tissue using methanol-facilitated solubilization and tryptic digestion coupled with 2D-LC-MS/MS. *Nat Protoc* **1**, 2784–2790 (2006).
- Griffin, N. M. *et al.* Label-free, normalized quantification of complex mass spectrometry data for proteomic analysis. *Nat Biotechnol* **28**, 83–89 (2010).



48. Szabo, E. & Colman, B. Isolation and characterization of carbonic anhydrases from the marine diatom *Phaeodactylum tricornerutum*. *Physiol. Plant.* **129**, 484–492 (2007).
49. Nielsen, E. S. The use of radio-active carbon ( $C^{14}$ ) for measuring organic production in the sea. *Journal du Conseil* **18**, 117–140 (1952).

## Acknowledgments

We thank Dr. Qiang Hu for valuable suggestions and helpful discussions of the manuscript. This work was supported by National Natural Science Foundation of China (41176137); the nonprofit research project for the State Oceanic Administration (201105008-2); Ministry of Science and Technology of the PRC fundamental research work (2012FY112900-01); 863 Project (2012AA100811-5).

## Author contributions

G.W. and W.G. conceived and designed the experiment. W.G., H.L., P.Z., R.Y. and S.G. conducted the experiments. G.W., W.G., G.P., A.H., L.H. and X.X. analyzed the data. G.W. and W.G. wrote the paper. All authors reviewed the manuscript.

## Additional information

**Supplementary information** accompanies this paper at <http://www.nature.com/scientificreports>

**Competing financial interests:** The authors declare no competing financial interests.

**How to cite this article:** Gu, W. *et al.* Quantitative proteomic analysis of thylakoid from two microalgae (*Haematococcus pluviialis* and *Dunaliella salina*) reveals two different high light-responsive strategies. *Sci. Rep.* **4**, 6661; DOI:10.1038/srep06661 (2014).



This work is licensed under a Creative Commons Attribution-NonCommercial-ShareAlike 4.0 International License. The images or other third party material in this article are included in the article's Creative Commons license, unless indicated otherwise in the credit line; if the material is not included under the Creative Commons license, users will need to obtain permission from the license holder in order to reproduce the material. To view a copy of this license, visit <http://creativecommons.org/licenses/by-nc-sa/4.0/>